EFFECT OF LIFSHITZ QUANTUM PHASE TRANSITIONS ON THE NORMAL AND SUPERCONDUCTING STATES IN CUPRATES

S.G. OVCHINNIKOV,[1,2] M.M. KORSHUNOV,[1,3,4] E.I. SHNEYDER[1,5]

[1]**L.V. Kirensky Institute of Physics, Siberian Branch of Russian Academy of Sciences**
(Krasnoyarsk 660036, Russia; e-mail: sgo@iph.krasn.ru)

[2]**Siberian Federal University**
(Krasnoyarsk 660041, Russia)

[3]**Max-Planck-Institut für Physik komplexer Systeme**
(D-01187 Dresden, Germany)

[4]**Department of Physics, University of Florida**
(Gainesville, Florida 32611, USA)

[5]**Reshetnev Siberian State Aerospace University**
(Akademgorodok 50, Krasnoyarsk 660036, Russia)

PACS 71.27.+a,71.18.+y, 74.25.Jb

We study the doping evolution of the electronic structure in the normal phase of high-T_c cuprates. The electronic structure and the Fermi surface of cuprates with a single CuO_2 layer in the unit cell like $La_{2-x}Sr_xCuO_4$ have been calculated by the LDA+GTB method in the regime of strong electron correlations (SEC) and compared to ARPES and quantum oscillations data. We have found two critical concentrations, x_{c1} and x_{c2}, where the Fermi surface topology changes. Following I.M. Lifshitz's ideas of the quantum phase transitions (QPT) of the 2.5-order, we discuss the concentration dependence of the low-temperature thermodynamics. The behavior of the electronic specific heat $\delta(C/T) \sim (x - x_c)^{1/2}$ is similar to the Loram and Cooper experimental data in the vicinity of $x_{c1} \approx 0.15$. In the superconducting state of cuprates, we consider both magnetic and phonon contributions to the d-wave pairing and found that there is no dominant mechanism of superconductivity. Magnetic and phonon contributions to the critical temperature are of the same order.

1. Introduction

Nowadays, high-T_c cuprates is the second most studied class of condensed matter after semiconductors. Both the nature of superconductivity and the abnormal pseudogap feature of the normal phase are not clear yet [1–9]. A lot of experimental data on the electronic structure have been obtained by ARPES that reveals the doping evolution of the Fermi surface (FS) from small arcs near $(\pi/2, \pi/2)$ at a small doping to the large FS around (π, π) at a large doping [10]. Quantum oscillations measurements in strong magnetic fields on the single crystals $YBa_2Cu_3O_{6.5}$ [11] and $YBa_2Cu_4O_8$ [12] have proved the existence of small hole pockets in the underdoped (UD) cuprates that looks as a contradiction to the ARPES arcs. This contradiction has been explained by the interaction between holes and spin fluctuations in the pseudogap state with the existing short-range antiferromagnetic (AFM) order [13–16]. It occurs that a part of the hole pocket related to the shadow band has a smaller quasiparticle (QP) lifetime due to the QP scattering on spin fluctuations. Recently, the VUV laser ARPES [17] has found a closed FS pocket in the UD La-Bi2201 with a small intensity at the shadow band part. The strong interaction of electrons with spin fluctuations is a general property of SEC systems and takes place not only in cuprates but also, e.g., in manganates [18].

The conventional LDA (local density approximation) approach to the electronic structure in the regime of SEC fails. Various realistic multiband models of a CuO_2 layer in cuprates in the low-energy region result in the effective Hubbard and $t - J$ models [19–23]. In the hybrid LDA+GTB scheme [24] that combines the LDA calculations of the multiband $p - d$ model parameters and the generalized tight-binding (GTB) treatment of SEC, the low-energy effective $t - t' - t'' - J^*$ model has been obtained from a microscopic approach with all parameters being calculated *ab initio*.

Small hole pockets in the UD case with area $\sim x$ appear in a theory considering the hole dynamics in the AFM spin background and have been obtained by the exact diagonalization [25] and the quantum Monte Carlo studies of finite clusters [26, 27], as well as by various variational and perturbation calculations for the infinite-

dimensional lattice [28–32]. Once the long-range AFM order disappears with doping, the electronic structure calculations in the paramagnetic phase results in the dispersion of the valence band with the top at (π, π) and the large FS [33]. Still there are apologists of the "universal metal dispersion" calculating the LDA band structure and the FS and claiming the rigid band behavior with a Fermi level shift of the fixed band dispersion [34]. After the small hole pockets were discovered in the Landau oscillations experiments [11, 12], the rigid band scenario becomes evidently unconvincing. In place of the conventional Fermi liquid state of a normal metal, the pseudogap state appears in the phase diagram of cuprates beside the long-range AFM phase. Though the origin of the pseudogap state is still debated, the contribution of the fluctuating short-range AFM order is clear [5]. The short-range AFM order is essential not only in the UD region. Even at the optimal doping, the AFM correlation length $\xi_{\rm AFM} \approx 10$ Å [35]. At low temperatures $T \leq 10$ K, spin fluctuations are slow with a typical time scale of 10^{-9} s and on the spatial scale of $\xi_{\rm AFM}$ (size of the AFM microdomain) [36]. This time is large in comparison with the fast electronic lifetime in ARPES ($\sim 10^{-13}$ s) [37] and the cyclotron period $T \sim 2\pi\omega_c^{-1} \sim 10^{-12}$, ω_c being a cyclotron frequency in quantum oscillations experiments [11, 12]. Thus, we safely consider that the spin fluctuations are frozen at low T and take only the spatial dependence of the short-range AFM order into account. This means that the electronic self-energy $\Sigma(k, \omega)$ will depends only on the momentum, $\Sigma(k, \omega) \to \Sigma(k)$.

We use this approach to study the concentration dependence of the electronic structure and the FS. In Section 2, we present the electronic structure and the change of the FS topology within the $t-t'-t''-J^*$ model. The FS area and the Luttinger theorem are also discussed. In Section 3, we give the qualitative picture based on the interaction between hole and spin fluctuations. In Section 4, we use the Lifshitz ideas [38, 39] on the QPT to study the low-temperature thermodynamics. The electronic specific heat singularity near a QPT is compared with the experimental data [40]. In Section 5, we extend the same approach to the superconducting d-wave state. We found that both magnetic and phonon contributions to T_c are similar in magnitude.

2. The Fermi Surface of $La_{2-x}Sr_xCuO_4$ and Its Doping Evolution

Within the LDA+GTB approach, we start from the *ab initio* LDA calculations and construct the Wannier functions in the basis of oxygen p-orbitals and copper e_g-orbitals. The multiband $p-d$ model [41] parameters are calculated *ab initio*. Then we apply the cluster perturbation approach [19, 42] and introduce the Hubbard X-operators constructed within the full set of eigenstates of the unit cell (a CuO_6 cluster) that is obtained by the exact diagonalization of the multiband $p-d$ model Hamiltonian of the cluster. By the GTB method, we construct the low-energy effective Hubbard model with $U = E_{\rm CT}$, where $E_{\rm CT}$ is the charge transfer gap [43]. In the Hubbard model, the $X_f^{0\sigma}$ operator describes the hole annihilation at the site f in the lower Hubbard band (LHB) of holes that corresponds to an electron at the bottom of the conductivity band. (Here, f enumerates the CuO_6 unit cells.) The hole annihilation in the upper Hubbard band (UHB) is given by the $X_f^{\bar{\sigma}2}$ operator and corresponds to an electron at the top of the valence band. In the limit of SEC, $U_{\rm eff} \gg t$ (t is the effective intersite hopping), we may exclude either the two-hole state $|2\rangle$, obtain the effective Hamiltonian for LHB describing the electron-doped cuprates or two-electron state $|0\rangle$ (hole vacuum $d^{10}p^6$), and get the effective Hamiltonian for UHB. The latter case is interesting for the hole-doped cuprates. We emphasize that the effective $t-t'-t''-J^*$ model is derived from the microscopic approach and its parameters are calculated *ab initio*. Here, J^* means that we take into account not only the superexchange interaction of localized spins J but also the 3-site correlated hopping that is of the same order as J and has to be included in the theory [45].

The model Hamiltonian is given by

$$H_{t-J^*} = H_{t-J} + H_{(3)},$$

$$H_{t-J} = \sum_{f,\sigma} \left[(\varepsilon - \mu) X_f^{\sigma\sigma} + (\varepsilon_2 - 2\mu) X_f^{22}\right] +$$

$$+ \sum_{f \neq g, \sigma} t_{fg}^{11} X_f^{2\bar{\sigma}} X_g^{\bar{\sigma}2} + \sum_{f \neq g} J_{fg} \left(\mathbf{S}_f \cdot \mathbf{S}_g - \frac{1}{4} n_f n_g\right)$$

$$H_{(3)} = \sum_{f \neq m \neq g, \sigma} \frac{t_{fm}^{01} t_{mg}^{01}}{U_{\rm eff}} \left(X_f^{\sigma 2} X_m^{\bar{\sigma}\sigma} X_g^{2\bar{\sigma}} - X_f^{\bar{\sigma}2} X_m^{\sigma\sigma} X_g^{2\bar{\sigma}}\right).$$

Here, $J_{fg} = 2\left(t_{fg}^{01}\right)^2 / U_{\rm eff}$, t_{fg}^{01} is the interband (LHB $\leftrightarrow$ UHB) hopping parameter between two sites f and g, $\mathbf{S}_f$ is the spin operator, ε and ε_2 are one- and two-hole local energies, and μ is the chemical potential. The intraband

hopping parameters t_{fg}^{11} have been calculated up to the 6-th nearest neighbors. It appears that only 3 coordination spheres are important. The dispersion with hoppings only to the nearest neighbors and to the next-nearest neighbors is qualitatively different from the dispersion calculated for 3 coordination speres. The contribution of the more distant neighbors to the hole dispersion is negligible. The parameters calculated *ab initio* within the model for $La_{2-x}Sr_xCuO_4$ are (in eV):

$$t = 0.932,\ t' = -012,\ t'' = 0.152,$$

$$J = 0.298,\ J' = 0.003,\ J'' = 0.007.$$

We introduce the hole Green function in the UHB (here, $\bar{\sigma} \equiv -\sigma$)

$$G_\sigma(\mathbf{k}, E) = \left\langle\left\langle X_{\mathbf{k}}^{\bar{\sigma}2} \middle| X_{\mathbf{k}}^{2\bar{\sigma}}\right\rangle\right\rangle_E . \tag{1}$$

The analysis of the whole set of diagrams in the X-operators diagram technique results in the exact generalized Dyson equation [44]

$$G_\sigma(\mathbf{k}, E) = \frac{\mathrm{P}_\sigma(\mathbf{k}, E)}{E - \varepsilon_0 + \mu - \mathrm{P}_\sigma(\mathbf{k}, E) t_{\mathbf{k}} - \Sigma_\sigma(\mathbf{k}, E)}.$$

Here, $t_{\mathbf{k}}$ is the Fourier transform of the hopping, $\mathrm{P}_\sigma(\mathbf{k}, E)$ and $\Sigma_\sigma(\mathbf{k}, E)$ are the strength and the self-energy operators. In the simplest Hubbard I approximation $\Sigma_\sigma = 0$, $\mathrm{P}_\sigma = F_{\bar{\sigma}2} = \langle X_f^{\bar{\sigma}\bar{\sigma}}\rangle + \langle X_f^{22}\rangle$. The QP spectral weight is determined by the filling factor $F_{\bar{\sigma}2}$. In the diagram technique, $F_{\bar{\sigma}2}$ corresponds to the so-called "terminal factors" [46].

To incorporate the effect of the short-range AFM order on the QP dynamics, we go beyond the Hubbard I approximation. The calculation scheme is given in [47]. We use the Mori-type method to project the higher order Green functions to the single particle function (1). A similar approach that took the spin dynamics into account was used in [23, 48]. The hole concentration in $La_{2-x}Sr_xCuO_4$ (LSCO) per unit cell is $n_h = 1 + x$. The completeness condition for the local Hilbert space in the $t - J$ model is

$$\sum_\sigma X_f^{\sigma\sigma} + X_f^{22} = 1.$$

Thus, we easily obtain $\langle X_f^{\sigma\sigma}\rangle = (1 - x)/2$, $\langle X_f^{22}\rangle = x$, and $F_{\bar{\sigma}2} = (1 + x)/2$. The Green function (1) becomes

$$G_\sigma(\mathbf{k}, E) = \frac{(1+x)/2}{E - \varepsilon_0 + \mu - \frac{1+x}{2} t_{\mathbf{k}} - \frac{1-x^2}{4} \frac{\left(t_{\mathbf{k}}^{01}\right)^2}{U_{\mathrm{eff}}} - \Sigma(\mathbf{k})}, \tag{2}$$

and the self-energy is given by

$$\Sigma(\mathbf{k}) = \frac{2}{1+x} \frac{1}{N} \sum_{\mathbf{q}} \Bigg\{ K(\mathbf{q}) \times$$

$$\times \left(t_{\mathbf{q}} - \frac{1-x}{2} J_{\mathbf{k}-\mathbf{q}} - x \frac{\left(t_{\mathbf{q}}^{01}\right)^2}{U_{\mathrm{eff}}} - \frac{(1+x)\, t_{\mathbf{k}}^{01} t_{\mathbf{q}}^{01}}{U_{\mathrm{eff}}} \right) + \frac{3}{2} C(\mathbf{q}) \times$$

$$\times \left(t_{\mathbf{k}-\mathbf{q}} - \frac{1-x}{2} \left(J_{\mathbf{q}} - \frac{(t_{\mathbf{k}-\mathbf{q}}^{01})^2}{U_{\mathrm{eff}}} \right) - \frac{(1+x) t_{\mathbf{k}}^{01} t_{\mathbf{k}-\mathbf{q}}^{01}}{U_{\mathrm{eff}}} \right) \Bigg\}.$$

Here, $K(\mathbf{q})$ and $C(\mathbf{q})$ stand for the Fourier transforms of the static kinetic and spin correlation functions,

$$K(\mathbf{q}) = \sum_{\mathbf{f}-\mathbf{g}} e^{-i(\mathbf{f}-\mathbf{g})\mathbf{q}} \left\langle X_{\mathbf{f}}^{2\bar{\sigma}} X_{\mathbf{g}}^{\bar{\sigma}2} \right\rangle ,$$

$$C(\mathbf{q}) = \sum_{\mathbf{f}-\mathbf{g}} e^{-i(\mathbf{f}-\mathbf{g})\mathbf{q}} \left\langle X_{\mathbf{f}}^{\sigma\bar{\sigma}} X_{\mathbf{g}}^{\bar{\sigma}\sigma} \right\rangle =$$

$$= 2 \sum_{\mathbf{f}-\mathbf{g}} e^{-i(\mathbf{f}-\mathbf{g})\mathbf{q}} \left\langle S_{\mathbf{f}}^z S_{\mathbf{g}}^z \right\rangle . \tag{3}$$

For the LHB which corresponds to the electron-doped cuprates, the similar Green function has been obtained previously [49]. We assume that the spin system is an isotropic spin liquid with any averaged component of the spin being zero and the equal correlation functions for any component of the spin, $\langle S_f^\alpha S_g^\alpha\rangle$, $\alpha = x,\ y,\ z$. We calculate this correlation function following [49] by the method developed previously for the Heisenberg model [50, 51]. The resulting static magnetic susceptibility agrees with the other calculations for the $t - J$ model [52, 53]. As for the kinetic correlation function, it is expressed via the same Green function (1).

The self-consistent treatment of the electronic and spin systems results in the evolution of the correlation functions (3), the chemical potential, and the FS as a function of the doping (Fig. 1). At a small doping, we get 4 hole pockets close to the $(\pi/2, \pi/2)$ point, as was expected for the AFM state. At the critical concentration $x_{c1} \approx 0.15$, the connection of these pockets appears along the $(\pi, 0) - (\pi, \pi)$ line, and the FS topology changes. At $x_{c1} < x < x_{c2} \approx 0.24$, we obtain two FS centered around the (π, π) point. The smaller one is the electronic FS; it shrinks with doping and collapses, when $x \to x_{c2}$. The larger one is the hole FS; with increasing x, it becomes more rounded. At $x > x_{c2}$, only a

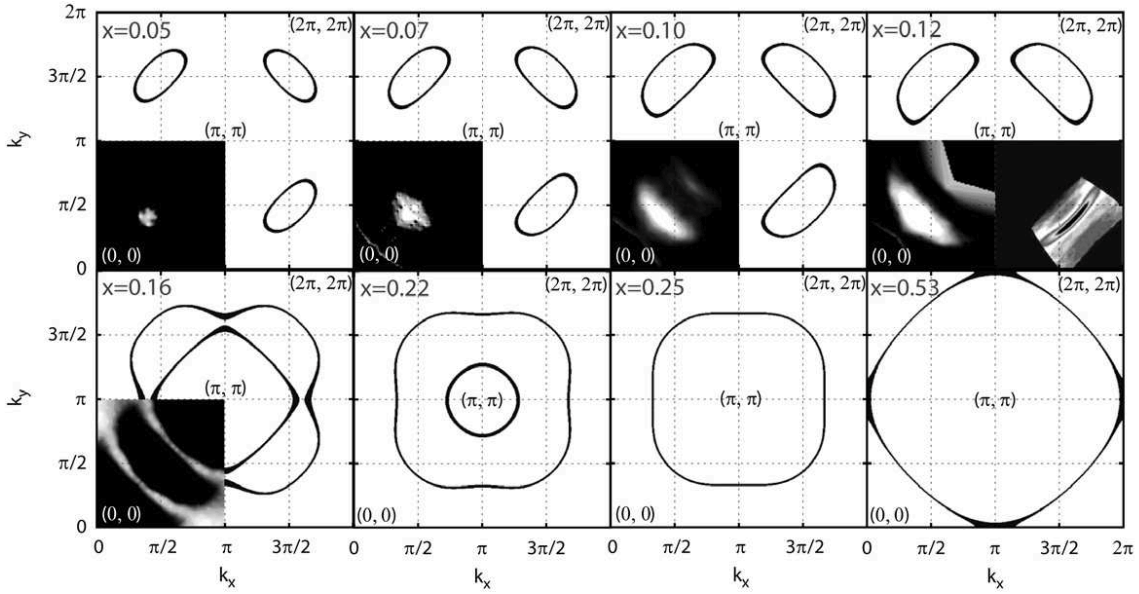

Fig. 1. Calculated Fermi surface for a single-layer cuprate for different doping levels x. Fermi surface topology changes at $x_{c1} = 0.15$ and $x_{c2} = 0.24$. ARPES data from [57] and [17] are shown in the lower left and lower right corners of the Brillouin zone, respectively

large hole FS remains. Finally, there is one more change of the topology at $x = x_{c3}$, when the FS touches the $(\pi, 0)$ point and becomes of the electronic type centered around the $(0, 0)$ point.

Note that the values of critical concentrations are obtained with a finite accuracy. First of all, the model parameters are deduced by a complicated procedure involving the projection of the LDA wave functions into the Wannier function basis and may vary with a change of this basis. Second, the equation for the Green function (2) is approximate and, with regard for higher order corrections, can change quantitatively values of the critical concentrations. On the other hand, the qualitative picture should remain unchanged, since it is due to the general properties of the electron scattering by AFM fluctuations. A qualitatively similar transformation of the FS with doping has been obtained within the Hubbard model in the regime of SEC (Fig. 15 in [48]), in the spin-density wave state of the Hubbard model [54], within the spin-fermion model [55], and in the *ab initio* multielectron quantum chemical approach [56]. The qualitative agreement of our results and the results of calculations in different approximations [48, 54–56] is basically due to the common underlying idea: the change of the electron dispersion caused by the interaction with the short-range AFM order. However, both magnetic and electronic properties are treated in our approach self-consistently.

In Fig. 1, we also show the ARPES data on $Bi_2Sr_{2-x}La_xCuO_{6+y}$ (Bi2201) from [57] and the recent data [17] on LSCO for doping concentrations of 0.10, 0.12, and 0.16. The single crystals of Bi2201 have been studied experimentally with different hole concentrations, $0.05 < p < 0.18$. This crystal has one CuO_2 layer in the unit cell. That is why our calculations appropriate for LSCO can be used for Bi2201 with the condition $x = p$. The question arises whether the model parameters are the same or different for the two crystals? In the conventional single electron tight-binding model used in [57] to fit the ARPES data, the hopping parameters depend on doping significantly. That is why the authors of [57] claim that the ratio t'/t is different for Bi2201 and LSCO. However, as evident from Figs. 5,*a* and 5,*b* of [57], the hopping values are close to each other for the lowest doping for both substances. The reason is that the hopping parameters depend on the interatomic distance that is almost the same in Bi2201 and LSCO. That is why we use the same parameters for all doping concentrations. The doping dependence of the band structure and its non-rigid behavior comes up as the effect of SEC. One of the main players in this game is the filling factor $F_{\bar{\sigma}2}$.

Comparing our calculated FS with the experimental data in Fig. 1, we notice that, for x =0.05, 0.07, 0.10, and 0.12, the experimental Fermi arc position is close to the calculated inner part of the hole pocket (the part which is near the $(0, 0)$ point). The outer part appears

as a low-intensity signal at $x = 0.10$ and $x = 0.12$ in ARPES. After the Lifshitz QPT at $x_{c1} = 0.15$, we see the two parts of the FS in agreement with ARPES data [57]. Usually, the outer FS (the nearest to (π, π) point) in Bicuprates is ascribed as the superlattice reflection. It may be that the superlattice signal simply masks a part of the FS that we obtain in the calculation. Another most probable explanation is that the scattering by AFM fluctuations suppresses the intensity of the spectral peaks corresponding to the outer FS. We will discuss this scenario in the next section.

At a higher doping, the ARPES results in a large hole pocket centered around the (π, π) point [58], e.g., in $Tl_2Ba_2CuO_{6+y}$ with $p = 0.26$. Our calculations result in such a topology for $x > x_{c2}$. According to [59], there is an electron pocket for LSCO at $x = 0.30$.

We now discuss the FS area and the Luttinger theorem. In Fig. 2, we give the FS area as a function of the doping. Note that the standard formulation of the Luttinger theorem does not work for Hubbard fermions. For free electrons, each quantum state in the k-space contains 2 electrons with opposite spins. The spectral weight of the Hubbard fermion is determined by the strength operator, $P_\sigma = F_{\bar{\sigma}2}$, and each quantum state contains $2F_{\bar{\sigma}2} = 1 + x$ electrons. A generalized Luttinger theorem for the SEC system [60] takes the spectral weight of each $|k\rangle$ state into account. For LSCO, the hole concentration $n_h = 1 + x$, so the electron concentration $n_e = 1 - x$. Using the dispersion law (see Fig. 3,*b* below), we calculate the number of occupied electronic states N_k^e below the Fermi level. The electronic concentration $n_e = 2F_{\bar{\sigma}2}N_k^e = 1 - x$. It gives us $N_k^e = (1 - x)/(1 + x)$. Then the number of free (occupied by holes) k-states is $N_k^h = 1 - N_k^e = 2x/(1 + x)$, and the FS area in Fig. 2 is determined by this number. The FS area obtained by the direct calculation of the occupied k-state under the Fermi level is shown by crosses. Two available FS areas from the quantum oscillations data [11, 12] are also marked in Fig. 2. It is evident and very important that the Luttinger theorem is not applicable in the standard formulation. On the other hand, its generalization for the case of correlated Hubbard fermions describes the experimental data very well.

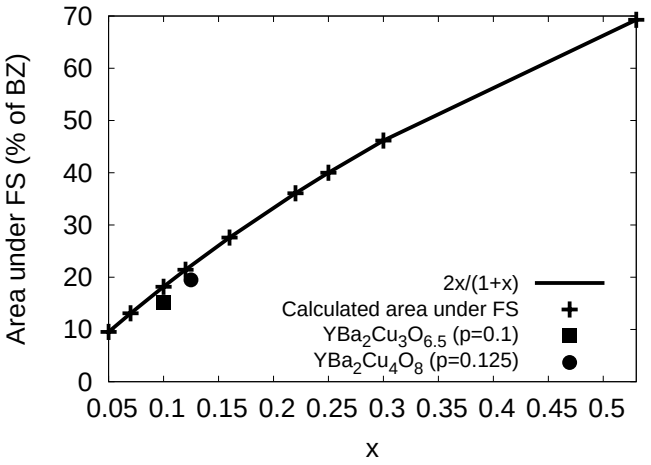

Fig. 2. Doping dependence of the FS area (in % of the Brillouin zone area) calculated directly (+) and from the generalized Luttinger theorem (solid line). The experimental values from the quantum oscillations data [11, 12] are shown as well

3. Qualitative Analysis of the Electron Dispersion and ARPES in a System with the Short-Range AFM Background

It was shown earlier [13–16] that AFM fluctuations transform the closed hole pocket into an arc. We will extent the same arguments to the doping region where AFM fluctuations are strong. The electron Green function on the square lattice with the electron scattering by Gaussian fluctuations that imitate the short-range AFM order with $Q = (\pi, \pi)$ is equal to [16]

$$G_D(\mathbf{k}, E) = \frac{E - \varepsilon(\mathbf{k} + \mathbf{Q}) + ivk}{(E - \varepsilon(\mathbf{k}))\,(E - \varepsilon(\mathbf{k} + \mathbf{Q}) + ivk) - |D|^2}. \tag{4}$$

Here, $|D|$ stands for the amplitude of the fluctuating AFM order, $\varepsilon(\mathbf{k})$ is the electron energy in the paramagnetic phase, and

$$v = |v_x(\mathbf{k} + \mathbf{Q})| + |v_y(\mathbf{k} + \mathbf{Q})|\,,\ v_{x,y}(\mathbf{k}) = \frac{\partial \varepsilon(\mathbf{k})}{\partial k_{x,y}}.$$

In the absence of the damping, the Green function (4) describes an electron in the spin-density wave state with the long-range order, where the Umklapp shadow band is given by $\varepsilon(\mathbf{k} + \mathbf{Q})$. On the other hand, there is a dynamical transition $\varepsilon(\mathbf{k}) \to \varepsilon(\mathbf{k} + \mathbf{Q})$ for the AFM spin-liquid with a finite lifetime $1/\tau \sim v\mathbf{k}$.

The paramagnetic dispersion is shown in Fig. 3,*a* by a thin green curve and a shadow band by a dotted curve to indicate that it has the finite lifetime as follows from Eq. (4). The resulting QP dispersion in the short-range AFM state is given by a thick blue curve. With increasing the doping, the Fermi level moves down from its initial value "0" in Fig. 3,*a*. The first intersection occurs along the $(0, 0) - (\pi, \pi)$ direction and results in 4 small hole pockets. The inner part of the FS is

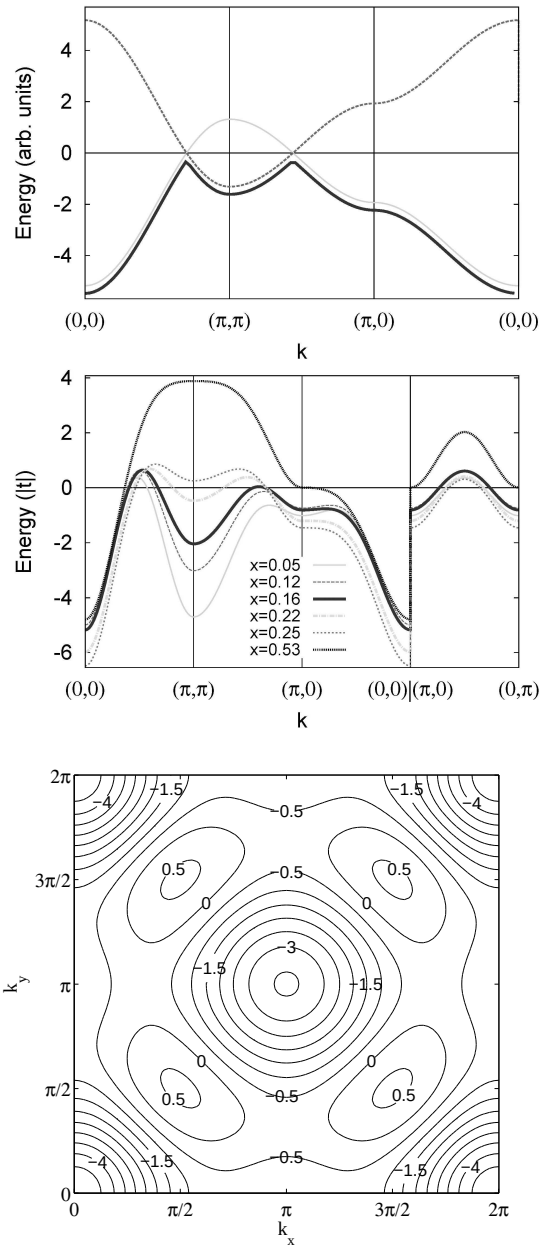

Fig. 3. Qualitative scheme of the band structure of an electron against the fluctuating AFM background (a), our calculations (*b*), and the constant-energy cuts for $x = 0.10$ (*c*). The zero energy in (*b*) and (*c*) corresponds to the Fermi level. The constant energy contours in (*c*) are labeled by the values of the corresponding energies (in units of t)

formed mainly by the non-damped electrons from the $\varepsilon(\mathbf{k})$ band, while the outer part is formed mainly by the damped shadow band. That is why the outer part has a very small spectral weight and was not seen in ARPES data until the recent discovery by the laser ARPES with the ultra-high energy resolution [17] (see Fig. 1). This qualitative analysis reproduce the calculations in [13–16, 48].

We now proceed to higher doping concentrations. For $x = 0.16$ where AFM correlation length $\xi_{\rm AFM} \approx 10$ Å, we have two large FS centered around (π, π). Those can be deduced from Fig. 3,*a* by a further decrease of the Fermi energy, μ. The critical point x_{c1} appears, when μ touches the second peak along the $(\pi, \pi) - (\pi, 0)$ direction. It is clear from Fig. 3,*a* that the inner FS will be of the electronic type and is formed by the damped shadow band. Thus, the corresponding spectral peaks are very small. The outer FS is of the hole type and is formed by the non-damped states. That is why its intensity is much larger than that of the inner part (see [57] and Fig. 1 for $x = 0.16$). With a further decrease of μ, it will cross the bottom of the band at $x = x_{c2}$, which corresponds to the collapse of the electronic FS. Finally, at $x > x_{c2}$, the crossing of μ with a saddle point at $(\pi, 0)$ results in the transformation of the FS from the hole to the electron type at $x = x_{c3}$. The latter takes place in a strongly OD regime; this effect can be obtained in any conventional single electron approach and has been discussed before [61]. For comparison, we present our calculated band structure for various doping concentrations in Fig. 3b and the constant energy cut in Fig. 3,*c*. It is clear that the rigid band approach of Fig. 3,*a* may give the correct sequence of the FS reconstruction, but it is quantitatively wrong.

4. Low Temperature Thermodynamics near the Lifshitz Transition

According to Lifshitz results [38, 39], both FS transformations at x_{c1} and x_{c2} are 2.5-order electronic phase transitions (nowadays, the term QPT is used). The appearance of a new FS sheet at $\varepsilon = \varepsilon_c$ gives the additional density of state $\delta g(\varepsilon) = \alpha(\varepsilon - \varepsilon_c)^{1/2}$, with $\alpha \sim 1$ in a 3D system. In spite of a strong anisotropy in cuprates, they are 3D crystals. The weak interlayer hopping results in a FS modulation along the k_z axis that has been measured by ARPES [34]. That is why we can use results of [38, 39] with a minimal modification due to the QP spectral weight in the strongly correlated system $F_{\bar{\sigma}2} = (1 + x)/2$.

Near the critical point, the thermodynamical potential gains additional contribution

$$\Omega(\mu, T) = \Omega_0(\mu, T) + \delta\Omega.$$

This singular contribution is induced by a new FS sheet at $\varepsilon > \varepsilon_c$ and is equal to

$$\delta\Omega = -\int_0^\infty \delta N(\varepsilon) f_F(\varepsilon) d\varepsilon,$$

where $f_F(\varepsilon)$ is the Fermi function. The number of states is given by

$$\delta N(\varepsilon) = \begin{cases} 0, & \varepsilon < \varepsilon_c \\ \frac{2}{3}\alpha\frac{1+x}{2}(\varepsilon-\varepsilon_c)^{3/2}, & \varepsilon > \varepsilon_c. \end{cases}$$

At low temperature, $T \ll z$, and $z = \mu - \varepsilon_c$. Near the QPT at $z = 0$, we get

$$\delta\Omega = \begin{cases} -\frac{\sqrt{\pi}}{4}(1+x)\alpha T^{5/2} e^{-|z|/T}, & z < 0, \\ -\frac{2}{15}(1+x)\alpha|z|^{5/2} - \frac{\pi^2}{12}(1+x)T^2|z|^{1/2}, & z > 0. \end{cases}$$

It is the $z^{5/2}$ singularity that tells about the 2.5-phase transition. In our case, z depends on the doping, so $z(x) = 0$ at $x = x_{c1}$ and $x = x_{c2}$.

The singular contribution to the Sommerfeld parameter $\gamma = C_e/T$, where C_e is the electronic specific heat, has the form

$$\delta\gamma = -\frac{\partial^2 \delta F}{\partial T^2} = \\ = \begin{cases} \frac{\sqrt{\pi}}{4}(1+x)\alpha\frac{|z|^2}{T^2}\left(1 + 3\frac{T}{|z|} + \frac{15}{4}\frac{T^2}{|z|^2}\right)e^{-|z|/T}, & z < 0, \\ \frac{\pi^2}{6}(1+x)\alpha z^{1/2}, & z > 0. \end{cases}$$

We have deduced the $z(x)$ dependence near each critical point from our band structure calculations. The obtained $\delta\gamma$ at $T = 10K$ near x_{c1} is shown in Fig. 4. We also plot the experimental data [40] for LSCO, where C_e has been obtained by extrapolation of the high temperature data for $T > T_c$ to the low-T region. The experimental points in Fig. 4 correspond to the total γ,

$$\gamma(x) = \gamma_0(x) + \delta\gamma,$$

where γ_0 is a smooth function at $x \approx x_{c1}$.

Since the electron FS pocket disappears for $x > x_{c2}$, our theory produces a singular behavior of $\gamma(x)$ for $x < x_{c2}$ corresponding to the case of $z > 0$. Measurements of the electronic specific heat [62] in $NdBa_2Cu_3O_{6+y}$ revealed two weak maxima of $\gamma(x)$ at $p = 0.16$ and $p = 0.23$ that are close to our x_{c1} and x_{c2}. To stay away from the superconductivity, the measurements in [62] were carried out at $T = 200K$, which explains why singularities appear as weak maxima.

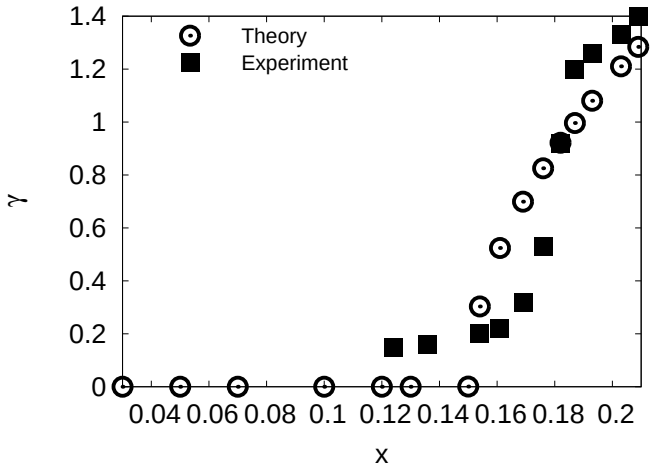

Fig. 4. Sommerfeld parameter near the Lifshitz QPT. Experimental data for $\gamma = C_e/T$ at $T = 10$ K were taken from [40]

5. Interplay of Magnetic and Phonon Contributions to *d*-Wave Pairing

A magnetic mechanism of pairing within the tJ model has been studied within various approaches. We use here the "no double occupation" constraint mean-field BCS-like version [23] and add the phonon contribution to the pairing. The resulting total coupling parameter is given by a sum of magnetic and phonon contributions [63]

$$\lambda_{\rm tot}(\mathbf{q}) = \frac{1-x}{2}J + \lambda_{\rm ph}\vartheta\left(|\xi_{\mathbf{q}} - \mu| - \omega_D\right),$$

where $\lambda_{\rm ph} = f(x)\,G$, $f(x) = (1+x)(3+x)/8 - 3C_{01}/4$ depends on the nearest neighbor spin correlation function $C_{01} < 0$, and G is the effective electron-phonon matrix element. The obtained doping dependence of T_c has maximum at the optimal doping $x_{c1} = 0.15$ due to the van Hove singularity in the density of states induced by the Lifshitz transition. This maximum of T_c results in a minimum of the isotope effect exponent. Fitting the calculated isotope effect exponent at the optimal doping to the experimental one, we found $G/J = 1.1$ and $T_c^{\max}(J \neq 0, G \neq 0) \approx T_c^{\max}(J = 0, G \neq 0)$ (see details in [64]). Thus, the phonon and magnetic contributions to T_c are of the same order of magnitude. This means that there is no dominant mechanism of pairing, both are equally important.

6. Conclusion

Previously, transformations of the FS has been discussed within a variational approach to the $t-J$ model [29]. The small hole pocket near the $(\pi/2, \pi/2)$ point has been obtained in the UD AFM. At a large doping, the electronic

FS around $(0,0)$ point also has been obtained. The same scenario of the FS evolution with doping was analyzed in the recent paper [65], where the authors considered the free dispersion of a doped antiferromagnet. Nevertheless, the FS for intermediate x in [29] does not correspond to our FS and to the experimental data in [17].

Recently, there were a lot of discussions on the change of the carrier sign upon doping. At large x, the FS becomes of the electronic type: in LSCO, this happens at $x > 0.30$ [66]. As was mentioned above, it is rather a trivial fact. More unusual are the experimental data on the change of the Hall coefficient ($R_{\rm H}$) sign in the UD systems. This effect was observed (under a strong magnetic field of $50 \div 60$T that suppresses the superconductivity) in $YBa_2Cu_3O_y$ with p =0.10, 0.12, and 0.14 [67], and in LSCO with $p = 0.11$ [68]. All these crystals belong to the region $x < x_{c1}$ and, according to our theory, should have the small hole FS pockets. We believe that the arguments of [69] can explain the negative total Hall coefficient due to opposite partial contributions to $R_{\rm H}$ of the FS with opposite curvatures in a two-dimensional metal.

The low-temperature transport measurements on $La_{1.6-x}Nd_{0.4}Sr_xCuO_4$ in a strong magnetic field up to 35T reveal a change of the FS topology at $p^* \approx 0.23$ [70]. This critical point is very close to our $x_{c2} = 0.24$. Also, our theory agrees with the data of [70] in the sense that, at $p = 0.24$, the R_H indicates the large cylindrical FS with $1+p$ holes. At $p = 0.20$ that corresponds to $x < x_{c2}$, the $R_{\rm H}(T)$ increase at a low temperature leads to the conclusion that the FS reconstruction and the pseudogap formation happen at $p < p^*$ [70]. The critical concentration x_{c2} agrees with the concentration $p_c = 0.23$, where the van Hove singularity in Bi2201 has been found in ARPES [71, 72].

There is a wide discussion in the literature on the quantum critical point $P_{\rm crit}$, where the pseudogap characteristic temperature $T^*(P) \to 0$. According to [73], $P_{\rm crit} = 0.19$, but $P_{\rm crit} = 0.27$ according to [74]. All these values are obtained by the extrapolation from a finite-T regime. On the contrary, the two critical points x_{c1} and x_{c2} obtained here are the properties of the ground state and result from the Lifshitz QPT. It is possible that our x_{c2} is somehow related to the $P_{\rm crit}$; at least, $p^* = 0.24$ is related to the pseudogap formation at $p < p^*$ [70].

We thank A. Kordyuk for the discussion of the results and T.M. Ovchinnikova for the technical assistance. This work was supported by project 5.7 of the programm "Quantum physics of the condensed matter" of the Presidium of the RAS, RFFI grant 09-02-00127, and integration project N 40 of SB RAS.

1. E. Dagotto, Rev. Mod. Phys. **66**, 763 (1994).
2. E.G. Maksimov, Phys. Usp. **43**, 965 (2000).
3. M. Imada, A. Fujimori, and Y. Tokura, Rev. Mod. Phys. **70**, 1039 (1998).
4. S.G. Ovchinnikov, Phys. Usp. **40**, 993 (1997).
5. M.V. Sadovskii, Phys. Usp. **44**, 515 (2001).
6. V.M. Loktev, R.M. Quick, S.G. Sharapov, Phys. Rep. **349**, 2 (2001).
7. V.F. Elesin, V.V. Kapaev, and Yu.V. Kopaev, Phys. Usp. **47**, 949 (2004).
8. Yu.A. Izyumov and E.Z. Kurmaev, Phys. Usp. **51**, 23 (2008).
9. P.A. Lee, Rep. Prog. Phys. **71**, 012501 (2008).
10. A. Damascelli, Z. Hussein, and Z.X. Shen, Rev. Mod. Phys. **75**, 473 (2003).
11. N. Doiron-Leyrand *et al.*, Nature **447**, 565 (2007).
12. E.A. Yelland, J. Singleton, C.H. Mielke, N. Narrison, F.F. Balakirev, B. Dabrowski, and J.R. Cooper, Phys. Rev. Lett. **100**, 047003 (2008).
13. E.Z. Kuchinskii, I.A. Nekrasov, M.V. Sadovskii, JETP Lett. **82**, 198 (2005).
14. E.Z. Kuchinskii and M.V. Sadovskii, JETP **103**, 415 (2006).
15. N. Harrison, R.D. McDonald, and J. Singleton, Phys. Rev. Lett. **99**, 206406 (2007).
16. E.Z. Kuchinskii and M.V. Sadovskii, JETP Lett. **88**, 192 (2008).
17. J. Meng, G. Liu, W. Zhang *et al.*, arXiv:0906.2682 (2009).
18. M.Yu. Kagan and K.I. Kugel, Phys. Usp. **44** 553 (2001).
19. S.G. Ovchinnikov and I.S. Sandalov, Physica C **161**, 607 (1989).
20. S.V. Lovtsov and V.Yu. Yushankhai, Physica C **179**, 159 (1991).
21. J.H. Jefferson, H. Eskes, and L.F. Feiner, Phys. Rev. B **45**, 7959 (1992).
22. V.I. Belinicher, A.L. Chernyshev, and V.A. Shubin, Phys. Rev. B **53**, 335 (1996).
23. N.M. Plakida and V.S. Oudovenko, Phys. Rev. B **59**, 11949 (1999).
24. M.M. Korshunov, V.A. Gavrichkov, S.G. Ovchinnikov, I.A. Nekrasov, Z.V. Pchelkina, and V.I. Anisimov, Phys. Rev. B **72**, 165104 (2005).
25. W. Stephan and P. Horsch, Phys. Rev. Lett. **66**, 2258 (1991).
26. R. Preuss, W. Hanke, and W. von der Linden, Phys. Rev. Lett. **75**, 1344 (1995).

27. V.F. Elesin and V.A. Koshurnikov, J. Exp. Theor. Phys. **79**, 961. (1994).
28. B.I. Shraiman and E.D. Siggia, Phys. Rev. Lett. **61**, 467 (1988).
29. S.A. Trugman, Phys. Rev. Lett. **65**, 500 (1990).
30. A.F. Barabanov, Superconductivity: Physics, Chemistry and Technology **3**, 8 (1990) (in Russian).
31. A.F. Barabanov, R.O. Kuzian, and L.A. Maksimov, J. Phys.: Condens. Matter. **39**, 129 (1991).
32. A.P. Kampf, Phys. Rev. **249**, 219 (1994).
33. G. Dorf, A. Muramatsu, and W. Hanke, Phys. Rev. B **41**, 9264 (1990).
34. S. Sahrakorpi, R.S. Markiewicz, H. Lin *et al.*, Phys. Rev. B **78**, 104513 (2008).
35. T.R. Thurston, R.J. Birgeneau, M.A. Kastner *et al.*, Phys. Rev. B **40**, 4585 (1989).
36. S.M. Haden *et al.*, Phys. Rev. Lett. **66**, 821 (1991).
37. D. Mihailovic and V.V. Kabanov, *Superconductivity in Complex Systems. Series: Structure and Bonding* Vol. **114**, edited by K. A. Müller and A. Bussmann-Holder (Springer, Berlin, 2005), p. 331.
38. I.M. Lifshitz, Sov. Phys. JETP **11**, 1130 (1960).
39. I.M. Lifshitz, M.Ya. Asbel, and M.I. Kaganov, *Electron Theory of Metals* (Consultants Bureau, New York, 1973).
40. J.W. Loram, J. Luo, J.R. Cooper, W.Y. Liang, and J.L. Tallon, Phys. Chem. Solids **62**, 59 (2001).
41. Ya.B. Gaididei, V.M. Loktev. Phys. Stat. Sol. B **147**, 307 (1988).
42. V.A. Gavrichkov, S.G. Ovchinnikov, A.A. Borisov, and E.G. Goryachev, JETP **91**, 369 (2000).
43. J. Zaanen, G.A. Sawatzky, and J.W. Allen, Phys. Rev. Lett. **55**, 418 (1985).
44. S.G. Ovchinnikov and V.V. Val'kov, *Hubbard Operators in the Theory of Strongly Correlated Electrons* (Imperial College Press, London, 2004).
45. V.V. Val'kov, T.A. Val'kova, D.M. Dzebisashvili, and S.G. Ovchinnikov, JETP Lett. **75**, 378 2002.
46. R.O. Zaitsev, Sov. Phys. JETP **41**, 100 (1975).
47. M.M. Korshunov and S.G. Ovchinnikov, Eur. Phys. J. B **57**, 271 (2007).
48. N.M. Plakida and V.S. Oudovenko, JETP **104**, 230 (2007).
49. V.V. Val'kov and D.M. Dzebisashvili, JETP **100**, 608 (2005).
50. H. Shimahara and S. Takada, J. Phys. Soc. Jpn **60**, 2394 (1991); **61**, 989 (1992).
51. A.F. Barabanov and V.M. Berezovskii, JETP **79** 627 (1994).
52. A. Sherman and M. Schreiber, Phys. Rev. B **65**, 134520 (2002).
53. A.A. Vladimirov, D. Ihle, and N.M. Plakida, Theor. Math. Phys. **145**, 1576 (2005).
54. S. Sachdev, A.V. Chubukov, and A. Sokol, Phys. Rev. B **51**, 14874 (1995).
55. A.F. Barabanov, A.A. Kovalev, O.V. Urusaev, A.M. Belemuk, and R. Hain, JETP **92**, 677 (2001).
56. L. Hozoi, M.S. Laad, and P. Fulde, Phys. Rev. B **78**, 165107 (2008).
57. M. Hashimoto, T. Yoshida, H. Yagi *et al.*, Phys. Rev. B **77**, 094516 (2008).
58. M. Plate, J.D.F. Mottershead, I.S. Elfimov *et al.*, Phys. Rev. Lett. **95**, 077001 (2005).
59. A. Ino, C. Kim, M. Nakamura *et al.*, Phys.Rev. B **65**, 094504 (2002).
60. M.M. Korshunov and S.G. Ovchinnikov, Phys. Sol. St. **45**, 1415 (2003).
61. F. Onufrieva and P. Pfeuty, Phys. Rev. B **61**, 799 (2000).
62. U. Tutsch, P. Schweiss, H. Wühl, B. Obst, and Th. Wolf, Eur. Phys. J. B **41**, 471 (2004).
63. E.I. Shneyder and S.G. Ovchinnikov, JETP Lett. **83**, 394 (2006).
64. E.I. Shneyder and S.G. Ovchinnikov, to be published in JETP (2009).
65. V.M. Loktev and V. Turkowski, J. Low Temp. Phys. **154**, 117 (2009).
66. I. Tsukada and S. Ono, Phys. Rev. B **74**, 134508 (2006).
67. D.Le Boeuf, N. Doiron-Leyraud, J. Levallois *et al.*, Nature **450**, 533 (2003).
68. T. Adachi, T. Noji, and Y. Koike, Phys. Rev. B **64**, 144524 (2001).
69. N.P. Ong, Phys. Rev. B **43**, 193 (1991).
70. R. Daou, N. Doiron-Leyrand, D. Le Boeuf *et al.*, Nature Phys. **5**, 31 (2009).
71. A. Kaminski, S. Rosenkranz, N.M. Fretweel *et al.*, Phys. Rev. B **73**, 174511 (2006).
72. A.A. Kordyuk, S.V. Borisenko, M. Khupfer, and J. Fink, Phys. Rev. B **67**, 064504 (2003).
73. J.G. Storey, J.L. Tallon, and G.V.M. Williams, Phys. Rev. B **78**, 140506(R) (2008).
74. S. Hufner, M.A. Hossain, A. Damascelly, and G.A. Sawatzky, Rep. Prog. Phys. **71**, 062501 (2008).

Received 20.09.09

ВПЛИВ КВАНТОВИХ ФАЗОВИХ ПЕРЕХОДІВ ЛІФШИЦА НА НОРМАЛЬНИЙ ТА НАДПРОВІДНИЙ СТАНИ КУПРАТІВ

С.Г. Овчинников, М.М. Коршунов, Е.І. Шнейдер

Р е з ю м е

У цій роботі обговорено зміни електронної структури в нормальній фазі високотемпературних надпровідників – шаруватих купратів. Результати розрахунків електронної структури та поверхні Фермі одношарових купратів методом LDA+GTB із врахуванням сильних кореляцій порівнюються з даними ARPES та квантових осциляцій. Виявлено дві критичні точки x_{c1} та x_{c2}, в яких відбувається перебудова поверхні Фермі. В околі критичних точок у межах ідеології І.М. Ліфшица про квантові фазові переходи 2,5 роду знайдено зміни термодинамічних властивостей за низьких температур. Особливість електронної теплоємності $\delta(C/T) \sim (x - x_c)^{1/2}$ достатньо добре узгоджується з відомими експериментальними даними в околі $x_{c1} \approx 0,15$. Якісно обговорюються зміни знака константи Холла з допуванням. Також розглянуто надпровідний стан з урахуванням магнітного і фононного механізмів спарювання.